

# Modeling the adhesive contact of rough soft media with an advanced asperity model

G. Violano<sup>1</sup> and L. Afferrante<sup>1,\*</sup>

*<sup>1</sup>Department of Mechanics, Mathematics and Management,  
Polytechnic University of Bari, Via E. Orabona, 4, 70125, Bari, Italy*

## Abstract

Adhesive interactions strongly characterize the contact mechanics of soft bodies as they lead to large elastic deformations and contact instabilities.

In this paper, we extend the Interacting and Coalescing Hertzian Asperities (ICHA) model to the case of adhesive contact. Adhesion is modeled according to an improved version of the Johnson, Kendall & Roberts (JKR) theory, in which jump-in contact instabilities are conveniently considered as well as the lateral interaction of the asperities and the coalescence of merging contact spots.

Results obtained on complex fractal geometries with several length scales are accurate as demonstrated by the comparison with fully numerical simulations and experimental investigations taken from the literature. Also, the model quite well captures the distributions of the contact stresses, gaps, and contact spots.

Keywords: Adhesion; rough contact mechanics; JKR theory, fractal surfaces.

---

\*Electronic address: [luciano.afferrante@poliba.it](mailto:luciano.afferrante@poliba.it)

## I. INTRODUCTION

Modeling adhesion between elastic media with rough surfaces is a demanding challenge. Bodies surfaces may be rough on several length scales, with roughness amplitudes ranging from nano to micrometric scale. Adhesion is of central importance in the design of high-technology devices, such as micro electromechanical systems (MEMS) [1], dry adhesives [2], stretchable electronics [3], biomimetic devices [4]. Moreover, adhesion plays a crucial role in the field of biomaterials, which are developed for drug delivery, medical diagnostics and tissue engineering [5]. More in general, tribological phenomena, e.g. friction and leak-rate of seals, are influenced by the presence of interfacial adhesion forces [6].

In this work, we focus on short-range type adhesion that is typical of soft elastic materials with high surface energy, where adhesion may lead to significative elastic deformations of the contacting bodies. In this range, the Johnson, Kendall & Roberts (JKR) theory [7], which assumes infinitely short-range adhesion, is widely believed to be valid.

Numerous authors developed theoretical and numerical approaches to study the adhesive contact mechanics of rough surfaces. In the framework of the JKR-type adhesion, we mention the work of Fuller & Tabor (FT) [8], who extended the Greenwood & Williamson (GW) multiasperity model [9] to the adhesive case. More recently, great progresses have been obtained with the multiscale theory of Persson [10, 11], where the detachment force is assumed proportional to an effective interfacial energy, and in brute-force numerical approaches [12], like those developed by Muser [13–15], where he shows that *”short-range adhesion compactifies contact patches, changes various microscopic distribution functions and enhances energy dissipation”*. Moreover, Rey et al. [16] with a FFT-based BEM methodology demonstrated that the coefficient of proportionality of the area-load relation increases with the surface energy.

In this work, adhesion is introduced in the Interacting and Coalescing Hertzian Asperities (ICHA) model [17, 18], according to the JKR theory, as modified in Ref. [19] to take into account jump into contact instabilities occurring when the local gap falls below a critical value. Experimental and numerical investigations showed that contact jumps are predominant in the adhesion of very soft bodies [20, 21] and are typically due to long-range adhesion interactions originally neglected in the JKR paper.

## II. THE MODEL

The fundamental equations of the JKR theory [7], which relate the contact load  $F$ , the contact radius  $a$ , and the contact approach  $\delta$ , are

$$F = \frac{4}{3} \frac{E^* a^3}{R} - \sqrt{8\pi E^* \Delta\gamma a^3} \quad (1)$$

$$\delta = \frac{a^2}{R} - \sqrt{\frac{2\pi a \Delta\gamma}{E^*}} \quad (2)$$

where  $R$  is the effective radius of curvature,  $E^*$  is the composite elastic modulus of the contacting bodies and  $\Delta\gamma$  is the interface adhesion energy.

The classical JKR model predicts the first contact occurs when the approach is zero and, hence, it neglects jump into contact instabilities. Wu [20] investigated the jump-in instability occurring in atomic force microscopy measurements, founding that jump-in is reached at a critical gap  $\Delta_{IN}$ . He proposed an empirical formula for the jump-in distance (valid for  $\mu \geq 2$ )

$$\Delta_{IN} = (1 - 2.641\mu^{3/7}) \epsilon \quad (3)$$

where  $\mu = \left(\Delta\gamma^2 R / E^{*2}\right)^{1/3} / \epsilon$  is the so-called Tabor parameter [22] and  $\epsilon$  is the range of attractive forces.

Ciavarella et al. [19], on the base of the Wu's findings, suggested to add the effect of van der Waals interactions in the JKR theory by using equation 3 for the jump-in critical distance.

Figure 1 shows how the JKR force-displacement relation modifies introducing the jump-in instability. During the loading phase, when  $\delta$  approaches the jump-in value  $\Delta_{IN}$ , snap-to-contact occurs at the point A and a sharp decrease in the contact force is observed (negative  $F$  corresponds to tensile force). During the unloading phase, when the approach  $\delta$  reduces up to the jump-off value  $\Delta_{OFF}$  (point C) unstable detachment occurs and the contact force and area vanish.

For randomly rough surfaces, multiple unstable jumps into contact are usually observed during the loading phase. Therefore, a multiasperity theory aimed at investigating the adhesive contact mechanics of soft media should take account of such phenomenon.

The *Interacting and Coalescing Hertzian Asperities* (ICHA) model, presented for the

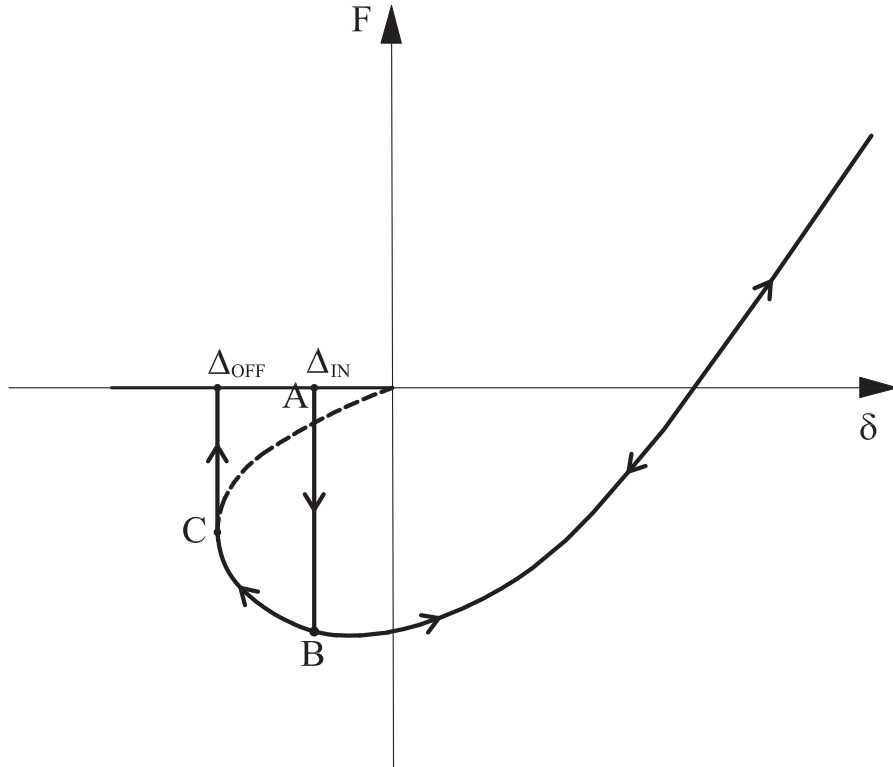


FIG. 1: The force-displacement relation as predicted by the JKR theory. The jump-in (point A) and jump-off (point C) are also showed.

first time in Ref. [17], is an advanced multiasperity based model, which showed to be quite accurate and efficient in predicting the main contact quantities of adhesiveless [12, 18] and DMT-type adhesive [23–25] rough contacts.

In presence of short-range adhesive interactions, DMT-type approaches fail. For this reason, here, we propose to introduce adhesion in the ICHA model according to the JKR theory, conveniently modified to also consider jump-in instabilities, as suggested in Ref. [19].

Consider a rigid rough media approaching to an elastic half-space. Following the JKR formalism, the normal displacement  $w_i$  of the elastic half-space at the location of the asperity  $i$  can be written as

$$w_i = \frac{a_i^2}{R_i} - \sqrt{\frac{2\pi a_i \Delta\gamma}{E^*}} + \hat{w}_i \quad (4)$$

where

$$\hat{w}_i = \sum_{j=1, j \neq i}^{n_{ac}} \frac{a_j^2}{\pi R_j} \left( \sqrt{\frac{r_{ij}^2}{a_j^2} - 1} + \left( 2 - \frac{r_{ij}^2}{a_j^2} \right) \arcsin \left( \frac{a_j}{r_{ij}} \right) \right) - \frac{1}{\pi a_j E^*} \sqrt{8\pi a_j^3 E^* \Delta\gamma} \arcsin \left( \frac{a_j}{r_{ij}} \right) \quad (5)$$

is the displacement due to the elastic interaction between all the asperities in contact  $n_{ac}$ . In eq. 5,  $r_{ij}$  is the distance between the asperities  $i$  and  $j$ .

The jump-in distance given in eq. 3 is calculated for each asperity. When the rough surface approaches the half-space, contact occurs when the gap between an asperity and the half-space becomes smaller than  $\Delta_{IN}$ . The first estimate of the asperity contact radius is done by inverting the JKR relation 2. Then, after a further increment of the approach  $\eta_i$ , the contact radius is increased by the quantity

$$\Delta a_i = \frac{\eta_i}{2a_i/R_i - \sqrt{\pi\Delta\gamma/(E^*a_i)}} \quad (6)$$

which is obtained by differentiating eq. 4.

The coalescence of merging contact patches is taken into account as described in Ref. [17]. Asperities with overlapping contact spots are replaced with a new equivalent one, which maintains the same total contact area of the suppressing asperities ( $a_{eq}^2 = a_i^2 + a_j^2$ ). Moreover, the position of the volume centroid is kept unchanged and the equivalent radius of curvature  $R_{eq}$  is empirically assumed as  $(R_i^2 + R_j^2)^{1/2}$ . Finally, the height  $h_{eq}$  of the new asperity is defined so that the contact area is effectively  $\pi a_{eq}^2$  at the given separation.

The total contact area and the total load are then obtained by summing up the contributions of all the asperities in contact.

Moreover, since a self-balanced load distribution is considered, the interfacial mean separation  $\bar{u}$  is computed as  $\bar{u}_0 - \delta$ , where  $\bar{u}_0$  and  $\delta$  are the initial separation and the total approach, respectively.

The local displacement at the location of a point  $Q$  outside the contact region can be

calculated as

$$w(Q) = \sum_{k=1}^{n_{ac}} \frac{a_k^2}{\pi R_k} \left( \sqrt{\frac{r_{Qk}^2}{a_k^2} - 1} + \left( 2 - \frac{r_{Qk}^2}{a_k^2} \right) \arcsin \left( \frac{a_k}{r_{Qk}} \right) \right) - \frac{1}{\pi a_k E^*} \sqrt{8\pi a_k^3 E^* \Delta\gamma} \arcsin \left( \frac{a_k}{r_{Qk}} \right) \quad (7)$$

where  $r_{Qk}$  is the distance between the asperity  $k$  and the point  $Q$ .

Moreover, as in the JKR theory adhesive stresses are supposed acting only inside the contact area  $\pi a^2$ , the contact pressure is obtained by superposing the Hertzian repulsive contribution and that due to a flat rigid cylindrical punch of the same radius  $a$ . Therefore, at distance  $r$  from the centre of the contact spot, the contact pressure is

$$p(r) = 2 \frac{E^* a}{\pi R} \left( 1 - \frac{r^2}{a^2} \right)^{1/2} - \left( 2 \frac{E^* \Delta\gamma}{\pi a} \right)^{1/2} \left( 1 - \frac{r^2}{a^2} \right)^{-1/2} \quad \text{for } r \leq a. \quad (8)$$

### III. ADHESION OF SELF-AFFINE FRACTAL SURFACES

The power spectral density (PSD) of natural surfaces often follows a self-affine behavior [26]. For this reason, we have performed calculations on nominally flat surfaces with roughness described by a self-affine fractal geometry with PSD

$$\begin{aligned} C(q) &= C_0 && \text{for } q_L \leq q < q_0 \\ C(q) &= C_0 (q/q_0)^{-2(H+1)} && \text{for } q_0 \leq q < q_1 \end{aligned} \quad (9)$$

Surfaces have been generated according to the spectral methodology developed in Ref. [27, 28].

In eq. 9,  $q$  is the modulus of the wave vector  $\mathbf{q} = (q_x, q_y)$ ,  $q_L = 2\pi/L$  (being  $L$  the lateral size of the domain) and  $q_1$  are the short and long frequencies cut-off, respectively, while  $q_0$  is the roll-off frequency. The exponent  $H$  is the *Hurst exponent*, which is related to the fractal dimension by  $D_f = 3 - H$ .

### A. Comparison with the Contact Mechanics Challenge's data

The Contact Mechanics Challenge (CMC) [12], proposed by Müser to the tribology community in 2015, consisted in simulating the adhesive contact between a rigid self-affine fractal surface and an elastic half-space. Several scientists participated submitting data obtained by their numerical, analytical and experimental methodologies.

One of the authors of this paper contributed with data obtained by the ICHA model; however, in that circumstance, the ICHA simulations were performed neglecting adhesion.

Since the parameters adopted in the CMC were chosen to mimic the short-range adhesion contact between a rubber and a polished surface, the conditions are close to the JKR limit. For this reason, one can expect that a JKR-like adhesion model is appropriate for studying the problem. Therefore, here we compare the results predicted by the proposed model with the reference data obtained with the Green Function Molecular Dynamics (GFMD) code by Müser [13, 14].

Fig. 2a shows, in a double-logarithmic plot, the normalized real contact area  $A/A_0$  as a function of the dimensionless pressure  $F/(E^*h'_{\text{rms}}A_0)$ , being  $A_0$  the nominal contact area and  $h'_{\text{rms}}$  the root mean square (rms) slope of the surface. Results show linearity in a large range of loads and the agreement with GFMD simulations is quite satisfactory.

In Fig. 2b the interfacial mean separation  $\bar{u}$ , normalized with respect to the rms roughness amplitude  $h_{\text{rms}}$ , is plotted as a function of dimensionless pressure  $F/(E^*h'_{\text{rms}}A_0)$ , in a double-logarithmic representation. Predictions of  $\bar{u}/h_{\text{rms}}$  with the ICHA model slightly exceed the reference solution, but once again the general trend is in good agreement.

Fig. 3a shows the gap probability distribution  $P(u)$  in a double-logarithmic chart. Results agree with the GFMD data with and without adhesion. Some discrepancies are observed only at low gaps. However, we observe that the accuracy of predictions is strongly influenced by the discretization of the surface mesh. In this respect, the solution shows the typical behavior of a short-range adhesion, which leads to a strongly reduced probability for small gaps. The latter is due to the formation of JKR adhesive necks near the contact line. To capture the formation of such necks, the calculations of the GFMD code were performed on systems with  $16 \times 10^9$  discretization points on the surface. The present simulations were instead carried out using only  $512 \times 512 = 262144$  grid points.

Fig. 3b shows the probability distribution of the dimensionless interfacial pressures

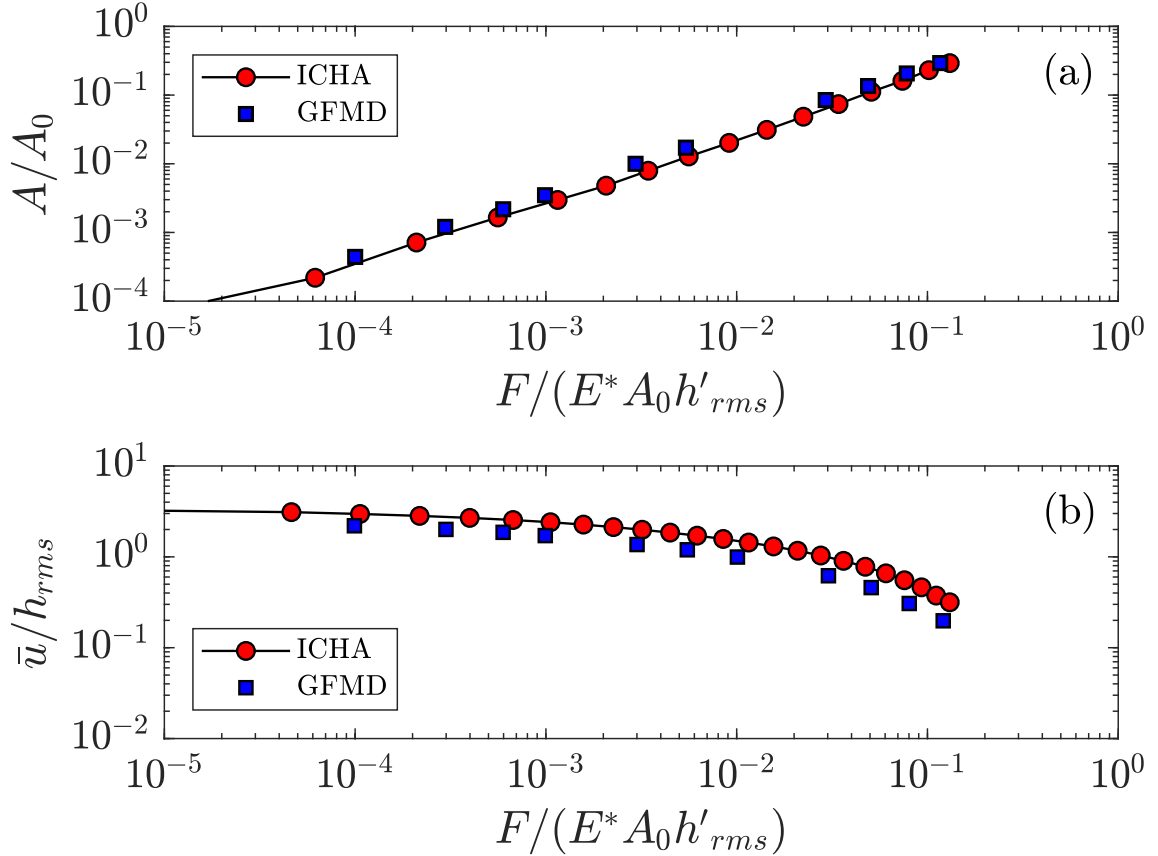


FIG. 2: (a): The normalized real contact area  $A/A_0$  as a function of the dimensionless load  $F/(E^* h'_{rms} A_0)$ . Results are referred to the ICHA model (red markers) and GFMD code (blue markers). (b): The normalized mean interfacial separation  $\bar{u}/h_{rms}$  as a function of the dimensionless load  $F/(E^* h'_{rms} A_0)$ . Results are referred to the ICHA model (red markers) and GFMD code (blue markers).

$P(p/(E^* h'_{rms}))$ . The lower number of discretization points could in part justify the differences observed at negative values of the pressure, where the ICHA model underestimates  $P(p/(E^* h'_{rms}))$ . Indeed, negative values of the pressure are expected at the edge of contact areas, i.e., at the location of JKR adhesive necks. Notice the pronounced peak at small negative pressures predicted in Ref. [12] and reflecting that "most non-contact points have an interfacial separation that greatly exceeds the range of the adhesive interaction", is absent in our simulations. In fact, the contribution to  $P(p/(E^* h'_{rms}))$  is originated only from contact regions as in our model stresses vanish in the non-contact points. For this reason, the comparison is proposed with the probability distribution originating from the true contact area.

Fig. 4 shows the contact spots predicted by the ICHA model (red circles) accurately

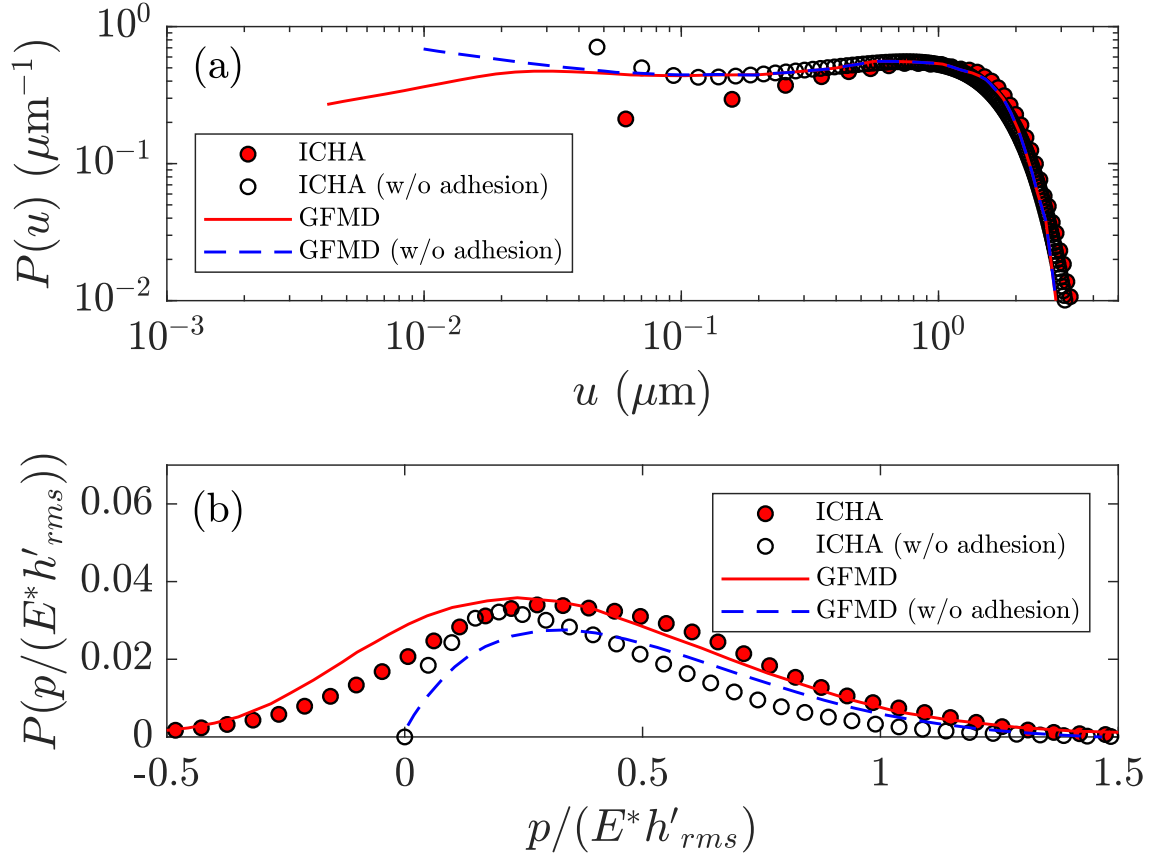


FIG. 3: (a): The gap probability distribution  $P(u)$ . Results are referred to the ICHA model with adhesion (red circular markers) and without adhesion (white circular markers), GFMD code without adhesion (blue dashed line) and GFMD code with adhesion (red solid line). (b): The probability distribution of the dimensionless interfacial pressures  $P(p/(E^* h'_{rms}))$ . Symbol details are the same of (a). Both in (a) and (b) results are obtained at a load  $F/(E^* h'_{rms} A_0) = 0.01$ .

follow the surface topography as they are located on the highest peaks of the surface (yellow regions).

## B. Comparison with the experimental measurements of McGhee et al.

McGhee et al. [29] measured the area-load relation in the contact between rough surfaces and smooth elastic PDMS samples. The CMC surface was produced on 1000 times scaled models with three different rms slopes  $h'_{rms} = 0.2, 0.5$  and  $1$ . Optical measurements of the contact area were performed using frustrated total internal reflectance. Moreover, different PDMS samples with various values of the composite elastic modulus  $E^*$  and surface energy  $\Delta\gamma$  were manufactured.

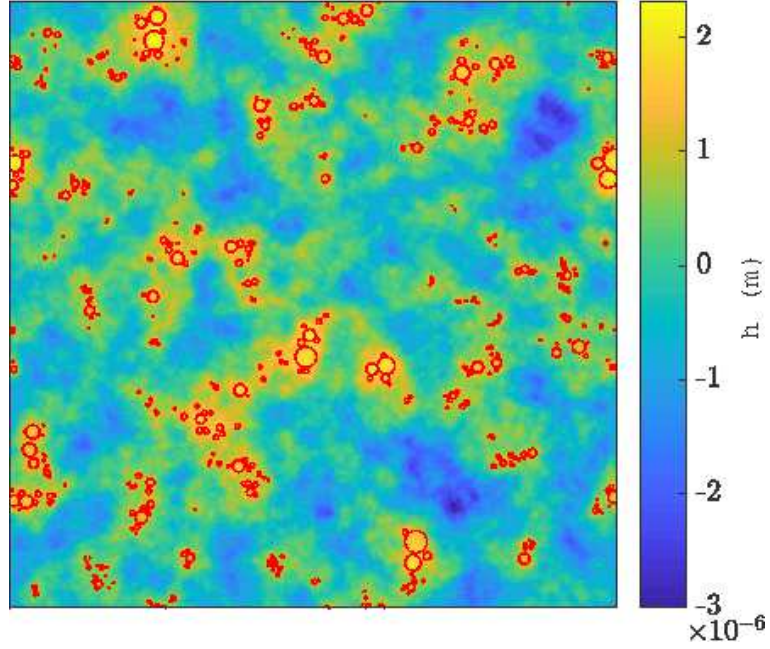


FIG. 4: The superposition of the contact spots predicted by the ICHA model (red circles) on the surface topography. Results are obtained at a load  $F/(E^*h'_{\text{rms}}A_0) = 0.01$ .

Fig. 5 shows a double-logarithmic representation of the normalized real contact area  $A/A_0$  as a function of the dimensionless pressure  $F/(E^*h'_{\text{rms}}A_0)$ . Results are presented for three values of  $E^*$  and  $\Delta\gamma$ , and at different values of the rms slope. The lines denote the experimental data taken from Ref. [29], while the markers correspond to the prediction of the ICHA model. A good agreement is observed for  $h'_{\text{rms}} = 0.5$  and 1. Some discordance occurs at  $h'_{\text{rms}} = 0.2$ , but we stress that for this value of the rms slope scattering was found in the experiments. Moreover, the manufactured surfaces do not truly satisfy the small-slope approximation as they were produced with the assigned rms gradient of one. Another potential “limitation” is the long-time viscoelastic response that can occur in the experiments.

Increasing the rms slope, a considerable decrease in the contact area is detected for a fixed value of the applied load. However, variations of the rms slope do not alter the shape of the contact patches under the condition of nearly equal contact area. A qualitative explanation of the former effects is proposed in Fig. 6, where the contact patches predicted by the ICHA model are shown for all the investigated values of  $h'_{\text{rms}}$ . In particular, results are shown at fixed dimensionless applied load  $F/(E^*A_0)$  (Fig. 6a) and normalized contact area  $A/A_0$  (Fig. 6b).

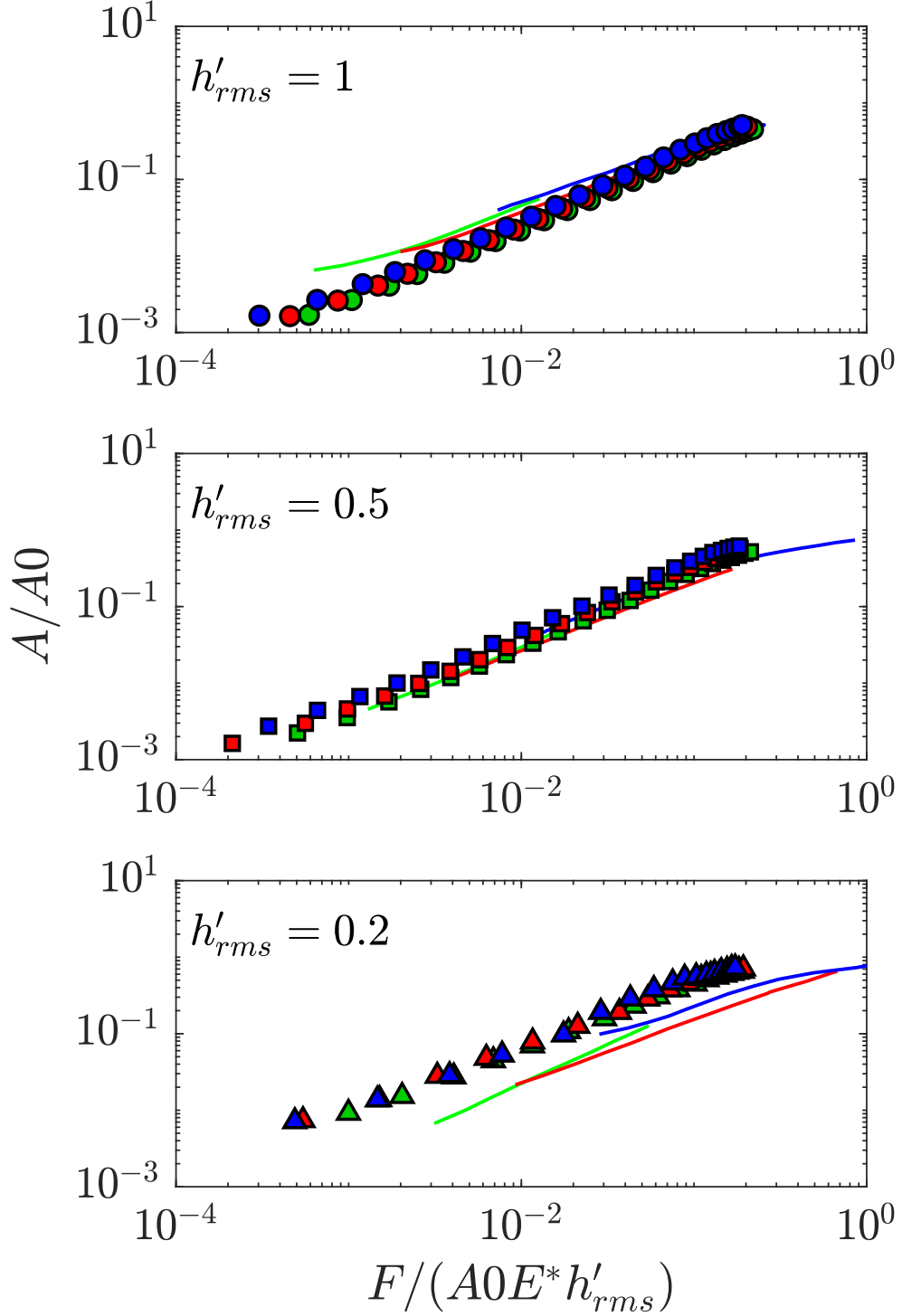


FIG. 5: The normalized real contact area  $A/A_0$  as a function of the dimensionless load  $F/(E^*h'_{rms}A_0)$ . We compare the ICHA model predictions (markers) and the experimental measurements of McGhee et al. (solid lines). Results are shown for three values of the rms slope  $h'_{rms} = 1$  (circles),  $h'_{rms} = 0.5$  (squares) and  $h'_{rms} = 0.2$  (triangles). Numerical and experimental investigations have been performed for different values of  $E^*$  and  $\Delta\gamma$ ; in particular we have used  $E^* = 0.24$  MPa,  $\Delta\gamma = 2$  mJ/m<sup>2</sup> (blue data),  $E^* = 0.75$  MPa,  $\Delta\gamma = 3$  mJ/m<sup>2</sup> (red data) and  $E^* = 2.10$  MPa,  $\Delta\gamma = 4$  mJ/m<sup>2</sup> (green data).

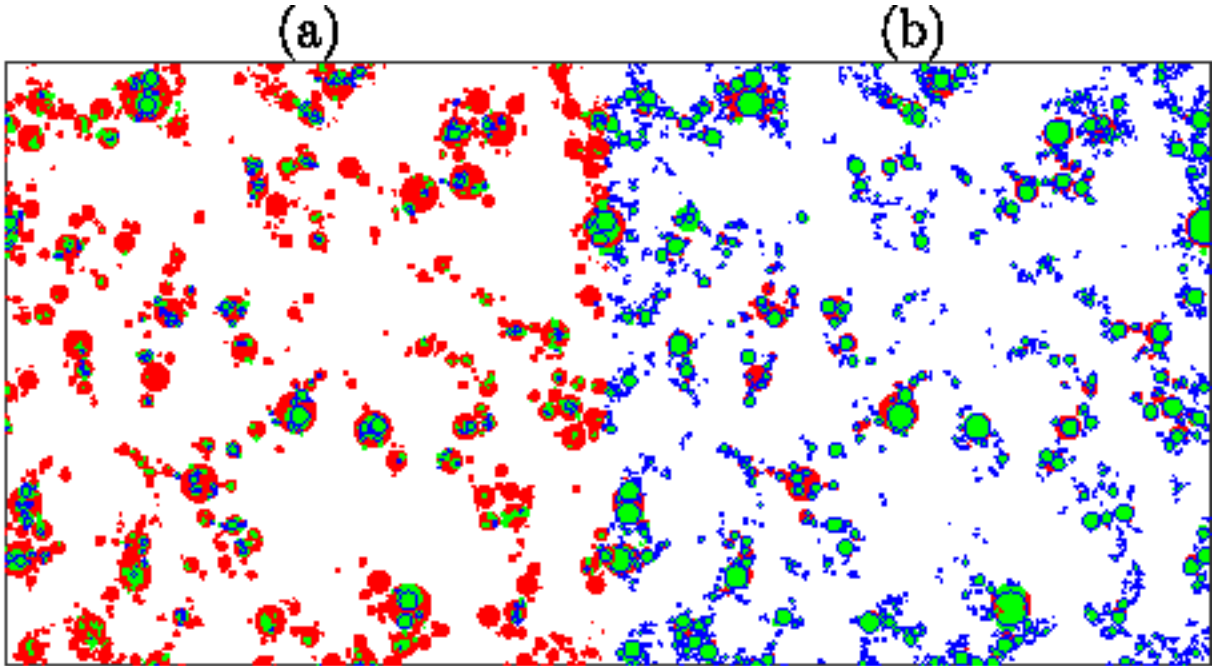


FIG. 6: The contact spots predicted by the ICHA model at fixed load (a) and fixed contact area (b) for three values of the rms slope  $h'_{\text{rms}} = 1$  (blue spots),  $0.5$  (green spots) and  $0.2$  (red spots).

#### IV. CONCLUSIONS

We have proposed an extension of the ICHA contact model to the case of short-range adhesion (JKR limit). In previous works, we have found such model to be accurate when adhesion is neglected or in the limit of contact with long-range adhesion (DMT limit). Here, the model confirms accuracy in predicting the main contact quantities as we infer from the comparison with data of the contact mechanics challenge [12] and experimental measurements [29].

Results show once again the fundamental role played by the elastic coupling and coalescence of merging contact spots as crucial factors to obtain good results with asperity models.

Hence, the ICHA model is fast as well as accurate in modeling adhesive contact problems; however, some limitations of the methodology are also evident as the adhesion of soft media inherently needs hard computational and time-consuming efforts for a better representation of the contact.

**Acknowledgement 1** *The authors acknowledge support from the Italian Ministry of Ed-*

- [1] Kim, S. H., Asay, D. B., & Dugger, M. T. (2007). Nanotribology and MEMS. *Nano today*, 2(5), 22-29.
- [2] Lin, P. C., Vajpayee, S., Jagota, A., Hui, C. Y., & Yang, S. (2008). Mechanically tunable dry adhesive from wrinkled elastomers. *Soft Matter*, 4(9), 1830-1835.
- [3] Morent, R., De Geyter, N., Axisa, F., De Smet, N., Gengembre, L., De Leersnyder, E., ... & Payen, E. (2007). Adhesion enhancement by a dielectric barrier discharge of PDMS used for flexible and stretchable electronics. *Journal of Physics D: Applied Physics*, 40(23), 7392.
- [4] Shah, G. J., & Sitti, M. (2004, August). Modeling and design of biomimetic adhesives inspired by gecko foot-hairs. In *2004 IEEE International Conference on Robotics and Biomimetics* (pp. 873-878). IEEE.
- [5] Shi, J., Votruba, A. R., Farokhzad, O. C., & Langer, R. (2010). Nanotechnology in drug delivery and tissue engineering: from discovery to applications. *Nano letters*, 10(9), 3223-3230.
- [6] Persson, B. N. J., Albohr, O., Tartaglino, U., Volokitin, A. I., & Tosatti, E. (2004). On the nature of surface roughness with application to contact mechanics, sealing, rubber friction and adhesion. *Journal of physics: Condensed matter*, 17(1), R1.
- [7] Johnson, K. L., Kendall, K., & Roberts, A. D. (1971). Surface Energy and the Contact of Elastic Solids. *Proceedings of the Royal Society A: Mathematical, Physical and Engineering Sciences*, 324(1558), 301–313. <https://doi.org/10.1098/rspa.1971.0141>
- [8] Fuller, K. N. G., & Tabor, D. (1975). The Effect of Surface Roughness on the Adhesion of Elastic Solids. *Proceedings of the Royal Society A: Mathematical, Physical and Engineering Sciences*, 345(1642), 327–342. <https://doi.org/10.1098/rspa.1975.0138>
- [9] Greenwood, J. A., & Williamson, J. B. P. (1966). Contact of Nominally Flat Surfaces. *Proceedings of the Royal Society A: Mathematical, Physical and Engineering Sciences*, 295(1442), 300–319. <https://doi.org/10.1098/rspa.1966.0242>
- [10] Persson, B. N. J., (2002). Adhesion between an elastic body and a randomly rough hard

- surface. *Eur. Phys. J. E.*, 8, 385–401. <https://doi.org/10.1140/epje/i2002-10025-1>
- [11] Persson, B. N. J., and Tosatti, E. (2001). The effect of surface roughness on the adhesion of elastic solids. *The Journal of Chemical Physics*, 115(12), 5597–5610. <https://doi.org/10.1063/1.1398300>
- [12] M. H. Muser, W. B. Dapp, R. Bugnicourt, P. Sainsot, N. Lesaffre, T. A. Lubrecht, B.N.J. Persson, K. Harris, A. Bennett, K. Schulze, S. Rohde, P. Ifju, W.G. Sawyer, T. Angelini, H.A. Esfahani, M. Kadkhodaei, S. Akbarzadeh, J.-J., Wu, G. Vorlaufer, A. Vernes, S. Solhjoo, A.I. Vakis, R.L. Jackson, Y. Xu, J. Streater, A. Rostami, D. Dini, S. Medina, G. Carbone, F. Bottiglione, L. Afferrante, J. Monti, L. Pastewka, M.O. Robbins, and J.A. Greenwood, (2017). Meeting the contact-mechanics challenge. *Trib. Letters*, 65, 118.
- [13] C. Campañá, M. H. Müser, Practical green’s function approach to the simulation of elastic semi-infinite solids, *Phys. Rev. B* 74 (2006) 075420.
- [14] N. Prodanov, W. B. Dapp, M. H. Müser, On the contact area and mean gap of rough, elastic contacts: Dimensional analysis, numerical corrections and reference data, *Tribol. Lett.* 53 (2014) 433–448.
- [15] Müser, M. H. (2016). A dimensionless measure for adhesion and effects of the range of adhesion in contacts of nominally flat surfaces. *Tribology International*, 100, 41–47. <https://doi.org/10.1016/j.triboint.2015.11.010>
- [16] Rey, V., Anciaux, G., & Molinari, J. F. (2017). Normal adhesive contact on rough surfaces: efficient algorithm for FFT-based BEM resolution. *Computational Mechanics*, 60(1), 69–81. <https://doi.org/10.1007/s00466-017-1392-5>
- [17] Afferrante, L., Carbone, G., & Demelio, G. (2012). Interacting and coalescing Hertzian asperities: A new multiasperity contact model. *Wear*, 278–279, 28–33. <https://doi.org/10.1016/j.wear.2011.12.013>
- [18] Afferrante, L., Bottiglione, F., Putignano, C., Persson, B. N. J., & Carbone, G. (2018). Elastic Contact Mechanics of Randomly Rough Surfaces: An Assessment of Advanced Asperity Models and Persson’s Theory. *Tribology Letters*, 66(2). <https://doi.org/10.1007/s11249-018-1026-x>
- [19] Ciavarella, M., Greenwood, J. A., & Barber, J. R. (2017). Effect of Tabor parameter on hysteresis losses during adhesive contact. *Journal of the Mechanics and Physics of Solids*, 98, 236–244.

- [20] Wu, J. J. (2010). The jump-to-contact distance in atomic force microscopy measurement. *The Journal of Adhesion*, 86(11), 1071-1085.
- [21] Greenwood, J. A. (1997). Adhesion of elastic spheres. *Proceedings of the Royal Society A: Mathematical, Physical and Engineering Sciences*, 453(1961), 1277–1297. <https://doi.org/10.1098/rspa.1997.0070>
- [22] Tabor, D. (1977). Surface forces and surface interactions. *Journal of Colloid And Interface Science*, 58(1), 2–13. [https://doi.org/10.1016/0021-9797\(77\)90366-6](https://doi.org/10.1016/0021-9797(77)90366-6)
- [23] Violano, G., & Afferrante, L. (2019). On DMT methods to calculate adhesion in rough contacts. *Tribology International*, 130, 36–42. <https://doi.org/10.1016/j.triboint.2018.09.004>
- [24] Violano, G., & Afferrante, L. (2019). Contact of rough surfaces: Modeling adhesion in advanced multiscale models. *Proceedings of the Institution of Mechanical Engineers, Part J: Journal of Engineering Tribology*, 1350650119838669.
- [25] Violano, G., Demelio, G. P., & Afferrante, L. (2018). On the DMT adhesion theory: from the first studies to the modern applications in rough contacts. *Procedia Structural Integrity*, 12, 58-70.
- [26] Persson, B. (2015). On the fractal dimension of rough surfaces. In *Fundamentals of Friction and Wear on the Nanoscale* (pp. 235-248). Springer, Cham.
- [27] Putignano, C., Afferrante, L., Carbone, G., & Demelio, G. (2012). A new efficient numerical method for contact mechanics of rough surfaces. *International Journal of Solids and Structures*, 49(2), 338–343. <https://doi.org/10.1016/j.ijssolstr.2011.10.009>
- [28] Putignano, C., Afferrante, L., Carbone, G., & Demelio, G. P. (2013). A multiscale analysis of elastic contacts and percolation threshold for numerically generated and real rough surfaces. *Tribology International*, 64, 148–154. <https://doi.org/10.1016/j.triboint.2013.03.010>
- [29] McGhee, A. J., Pitenis, A. A., Bennett, A. I., Harris, K. L., Schulze, K. D., Urueña, J. M., ... & Sawyer, W. G. (2017). Contact and deformation of randomly rough surfaces with varying root-mean-square gradient. *Tribology Letters*, 65(4), 157.